

Halloysite Nanotubes-Induced Al Accumulation and Fibrotic Response in Lung of Mice after 30-Day Repeated Oral Administration

Xue Wang, Jiachun Gong, Rui Rong, Zongxiang Gui, Tingting Hu, and Xiaolong Xu*

Department of Chemistry, University of Science and Technology of China, Hefei, 230026, P. R. China

ABSTRACT: Natural halloysite ($\text{Al}_2\text{Si}_2\text{O}_5(\text{OH})_4 \cdot n\text{H}_2\text{O}$) nanotubes (HNT) are clay materials with hollow tubular structure and are widely applied in many fields. Many *in vitro* studies indicate that HNTs exhibit a high level of biocompatibility; however, the *in vivo* toxicity of HNTs remains unclear. In this study, the biodistribution and pulmonary toxicity of the purified HNTs in mice were investigated after intragastric administration for 30 days. HNTs have high stability in biological conditions. Oral administration of HNTs caused significant Al accumulation predominantly in the lung with relative slight effects on Si biodistribution. Oral administration of HNTs stimulated the growth of the mice at low dose (5 mg/kg BW) with no pulmonary toxicity but inhibited the mouse growth and resulted in oxidative stress and inflammation in lung at high dose (50 mg/kg BW). In addition, oral HNTs at high dose could be absorbed from the gastrointestinal tract and deposited in lung and could also induce pulmonary fibrosis.

KEYWORDS: halloysite nanotubes, nanotoxicity, aluminum, lung, fibrosis

INTRODUCTION

Natural HNTs are a clay material with tubular structure having aluminum oxide octahedrons inside and silicon dioxide tetrahedrons outside.¹ Their lengths are from 200 nm to 15 μm , and their outer and inner diameters are 40–70 nm and 10–40 nm, respectively. HNTs have an extensive application in loading of different active agents due to their tubular structure.^{2,3} They are called “green” materials due to their high thermal stability, nanoscale tubular structure, low price, abundant deposition, and good biocompatibility. HNTs have been traditionally applied in polymeric composite and ceramics industries,^{4,5} water purification,⁶ as well as catalyst supports.^{7,8} Recently, scientists have developed various novel applications of HNTs in cosmetics, teeth fillers, bone implants, ultrasound contrast agents, cancer cell isolation, and drug carrier.^{9–12} In addition, HNTs, as food packaging materials^{13,14} and feed additives,^{15,16} have a potential application in food and feed industry, owing to their antimicrobial property.

Annually, about 30 thousand tons of halloysite minerals are mined in the world and processed into nanotubes.¹⁷ The wide applications of HNTs result in their release into the natural surroundings, because industrial uses could cause emissions of nanoparticles into the hydrosphere, atmosphere, or geosphere.^{18,19} HNTs are commonly found in natural water and soils.²⁰ Considering its potential stressor on the environment, it is necessary to evaluate the effects on plants and animals for developing a diversity of HNT applications. *In vitro* toxicities of HNTs have been widely reported. Cytotoxicity studies on five cell lines including HeLa, MCF-7, Caco-2/HT29-MTX, HCT116, and HepG2 have revealed that HNTs exhibited a high degree of biocompatibility.^{21–23} Currently, only a few *in vivo* investigations have been conducted to examine the toxicity of HNTs in plants and animals. Bellani et al.²⁴ have reported that HNTs are not phytotoxic to *Raphanus sativus L.* It was found that HNTs were safe for *Caenorhabditis elegans* at 1 mg/mL²⁵ and for *P. caudatum* at even higher concentration of 10

mg/mL.²⁶ However, the toxicity of HNTs in mammals is still unclear.

Usually, the commercially available HNTs are inhomogeneous in tube length and diameters and are impure with other matters, such as kaolinite and quartz.²⁷ It is reported that the toxicity associated with nanoparticles depends on the presence of impurities.²⁸ HNT are nanoparticles and the impurities in HNTs may affect their toxicity in animals. Recently, we have developed a method to purify HNTs.²⁷ This study attempts to assess the stability and biodistribution of the purified HNTs employing mammals, Kunming mice, as an animal model by oral route. The results showed that the majority of Al accumulated predominantly in the lung, while only a few of Al accumulated in the liver, kidney and spleen. Therefore, further investigation was carried out on HNTs-induced pulmonary toxicity and attempt was made to provide insight into whether the particles of oral HNTs were absorbed by the gastrointestinal tract and reached the lung.

MATERIALS AND METHODS

Materials. Raw halloysite powders were bought from Yan-Bo Minerals Processing Company (He Bei, China) and purified as described previously.²⁷ The purified HNTs were analyzed by transmission electron microscopy (TEM) (JEM-2010, JEOL Ltd., Japan) and sequential X-ray fluorescence (XRF) spectroscopy (XRF-1800, Shimadzu, Japan). A dynamic light scattering instrument (DLS) (Zetasizer, Malvern Instruments Ltd., U.K.) was used to determine the hydrodynamic diameter of HNTs.

Assays for Stability of HNTs in Biological Conditions. HNTs (1 mg/mL) were incubated with artificial gastric fluid (AGF) (34 mM NaCl, 0.32% pepsin, pH 1.50), artificial intestinal fluid (AIF) (420 μM trypsin, 50 mM KH_2PO_4 , pH 6.80) or artificial blood solution (ABS)

Received: October 5, 2017

Revised: February 7, 2018

Accepted: February 22, 2018

Published: February 22, 2018

($10 \mu\text{M}$ BSA, 137 mM NaCl, 2.7 mM KCl, 8 mM Na_2HPO_4 , 1.5 mM KH_2PO_4 , and pH 7.40) with gentle shaking at 37°C . After incubation for different times, the supernatant was obtained by centrifugation for 25 min at $15\,000\text{g}$. The contents of Al and Si in supernatants were measured by inductively coupled plasma-atomic emission spectrometry (ICP-AES) (Optima 7300DV, PerkinElmer).²⁹

Treatment of Animals. The 7 week-old Kunming male mice ($22.1 \pm 1.9 \text{ g}$, Animal Center of AMU, China) were acclimatized for 7 days in the condition as described previously.³⁰ Thirty male mice were divided randomly into one control group (saline solution) and two test groups ($5, 50 \text{ mg HNTs/kg body weight (BW)/day}$). The doses of HNTs were used following OECD Test Guideline 420.³¹ The mice were intragastrically injected with chemicals every day for 30 days. Mice were observed daily for any behavioral abnormalities and weighed every other day. After the last injection, the mice were fasted 12 h and then sacrificed after anaesthetization with ether. The blood was collected in time, and then the brain, kidney, lung, spleen, liver, and heart were dissected out. All experiments were performed in compliance with the approval of the Animal Ethical Committee of USTC and the guidelines of USTC for the care and use of laboratory animals.

Biodistributions of Al and Si. The brain, kidney, lung, spleen, liver, and heart tissues (about 0.2 g) were digested with HNO_3 using the method as described previously.³⁰ The contents of Al and Si in the resulting solution were measured with ICP-AES.

Histopathological Test. Lung tissues were harvested and immediately fixed in 10% formalin for 1 day and then embedded in paraffin. The sections ($5 \mu\text{m}$) were stained with hematoxyline and eosine and imaged by an optical microscope (IX-81, Olympus, Japan).

Confocal Raman microscopy. Raman spectra of lung sections were determined in backscattering geometry in a confocal configuration using a LABRAM-HR Raman microscope system equipped with a 785 nm semiconductor laser (JY Co. in Fort-de-France, Martinique) at room temperature. The integration time was 1 s. Laser resolution and power were $0.3 \pm 0.1 \text{ cm}^{-1}$ and 80 mW, respectively. The lung specimen was embedded in paraffin, sliced into $5 \mu\text{m}$ thickness, and then placed on a glass slide. The slide was stained with hematoxyline and eosine and then scanned by the confocal Raman microscope.

Oxidative Stress Assay. Oxidative biomarkers of lung tissues were analyzed by the previous methods.³⁰ The level of malondialdehyde (MDA) and the activities of glutathione peroxidase (GSH-Px) and superoxide dismutase (SOD) were determined by commercial kits (Nanjing Jiancheng Bioeng Inst., China), according to the instructions of the manufacturer.

Cytokine Expression Assay. The cyclooxygenase-2 (COX-2) and nitric oxide synthase (iNOS) levels in mouse lung tissues were determined by ELISA using commercial kits (Shanghai Jianglai Biotechnology Co., Ltd., Shanghai, China), following the manufacturer's instructions. The absorbances of all samples (iNOS and COX-2) were detected at 450 nm on a microplate reader (Bio-Tek, ELX-800, Vermont). A standard curve was used to calculate the concentrations of iNOS and COX-2 for each sample.

Statistical Analysis. SPSS 19.0 (SPSS Inc., Chicago, IL) was used to analyze the data by one-way analysis of variance test. Dunnett's test was used to compare the differences between the control group and the particle groups. The statistical significance was set at $p < 0.05$ for all tests.

RESULTS

Characterization of Purified HNTs. The purified HNTs were obtained by the previous methods.²⁷ The homogeneities and sizes of purified HNTs and raw HNTs were characterized by TEM. A broad peak of distribution was observed for raw HNTs ranging from 60 to 950 nm (Figure 1A,C). The purified HNTs had good dispersity with high homogeneity and less impurities, the average length of which was $180 \pm 8 \text{ nm}$ (Figure 1B,D). The average inner and outer diameters of

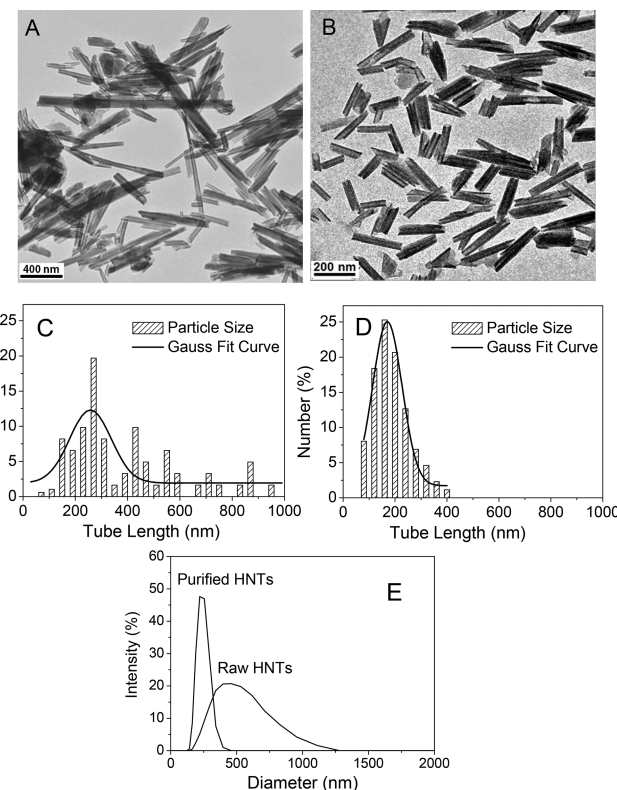


Figure 1. Characterization of purified HNTs. TEM images of raw (A) and purified (B) HNTs. (C) Size distribution profile of raw HNTs (the number of analyzed particles, 465) measured by TEM. (D) Size distribution profile for purified HNTs (the number of analyzed particles, 382) measured by TEM. (E) Size distributions of raw (1) and purified (2) HNTs in physiological saline solution measured by DLS.

purified HNTs were $14.6 \pm 1.3 \text{ nm}$ and $40.2 \pm 3.1 \text{ nm}$, respectively, and their average aspect ratio was 4.5 ± 0.3 . The results of DLS measurements showed that raw HNTs had a broad size distribution peak, with the average diameter of $436 \pm 14 \text{ nm}$ (Figure 1E). The purified HNTs had a rather sharp size distribution peak, with an average diameter of $229 \pm 8 \text{ nm}$. It was larger than those determined by TEM because of the effects of the adsorbed stabilizer (hexadecyl trimethylammonium bromide) on the nanotube surface.²⁷ The elemental analysis indicated that many other elements (S, Mg, Ca, K, Fe, Na, P, Ti, Sr, Mn, Zr, and Ni) existed in the raw HNTs (Table 1). The impurities of K_2O , TiO_2 , SrO , MnO , NiO , and ZrO_2 were removed from the HNTs and the Fe and S levels markedly decreased after purification. The purified HNTs were used in this study to evaluate their stability in biological conditions and their toxicity in mice.

Stability of HNTs in Biological Conditions. The stability of HNTs in AGF, AIF, and ABS were measured by ICP-AES. As shown in Figure 2A, only 0.62% of Al ions and 0.64% of Si ions in HNTs were released into AGF after 4 h, revealing the high stability of HNTs in AGF. As shown in Figure 2B,C, HNTs were much more stable in ABS or AIF than in AGF, suggesting that the pH value of the solution affected the dissolution of Al and Si ions in HNTs. The results also suggest that both Al and Si ions were dissolved from HNTs at similar rates in AGF. However, compared with Si ions, Al ions were released from HNTs at a much lower rate in AIF or ABS,

Table 1. Components of Purified and Raw HNTs by Sequential X-ray Fluorescence (XRF)

chemistry (wt %)	raw HNTs	purified HNTs
SiO ₂	55.88	59.89
Al ₂ O ₃	32.09	35.20
Fe ₂ O ₃	4.17	2.66
SO ₃	4.40	0.84
K ₂ O	1.11	not detected
MgO	0.48	0.45
CaO	0.79	0.61
TiO ₂	0.39	not detected
P ₂ O ₅	0.10	0.03
Na ₂ O	0.40	0.32
NiO	0.03	not detected
MnO	0.06	not detected
SrO	0.07	not detected
ZrO ₂	0.03	not detected

suggesting that the dissolution rate of Al ions was much less than that of Si ions at pH 6.8 or 7.4.

Biodistributions of Al and Si. HNTs are natural aluminosilicates that contain Al and Si. To identify the main target organs of oral HNTs in mice, the biodistributions of Al and Si were determined by ICP-AES after oral administration of HNTs at 50 mg/kg BW for 7 days. Figure 3A shows that majority of Al accumulated predominantly in the lung, while only a few of Al accumulated in the spleen, kidney, and liver. However, only a few of Si accumulated in the lung (Figure 3B). Slight Si accumulations were also found in the liver, kidney, and spleen. The marked Al accumulation in the lung revealed that the main target organ of oral HNTs was the lung. Park et al. also found that majority of Al accumulated predominantly in

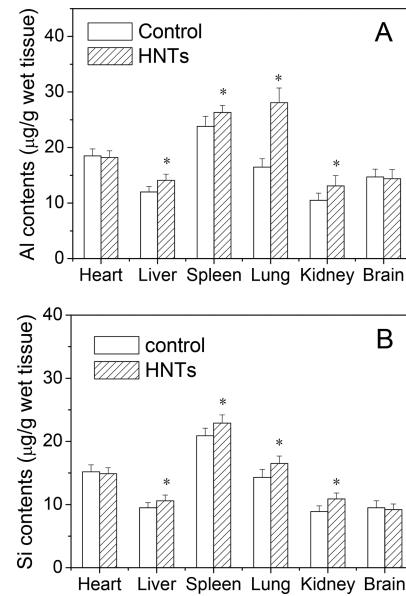


Figure 3. Biodistributions of Al (A) and Si (B) in the mouse tissues measured with ICP-AES. The mice were orally administrated with HNTs at 300 mg/kg BW for 7 days. Data are shown as means \pm SD, $n = 4$. * $p < 0.05$ versus the control.

the mouse lung after repeated oral administration of Al₂O₃ nanoparticles at 60 mg/kg for 28 days.³² Therefore, further investigation of the pulmonary toxicity caused by oral HNTs was done for 30 days at the two doses (5, 50 mg/kg BW).

Body Weight and Lung Coefficient. During the period of the 30-days experiments, no animals showed any abnormal symptoms in the control or low dose (5 mg/kg BW) group,

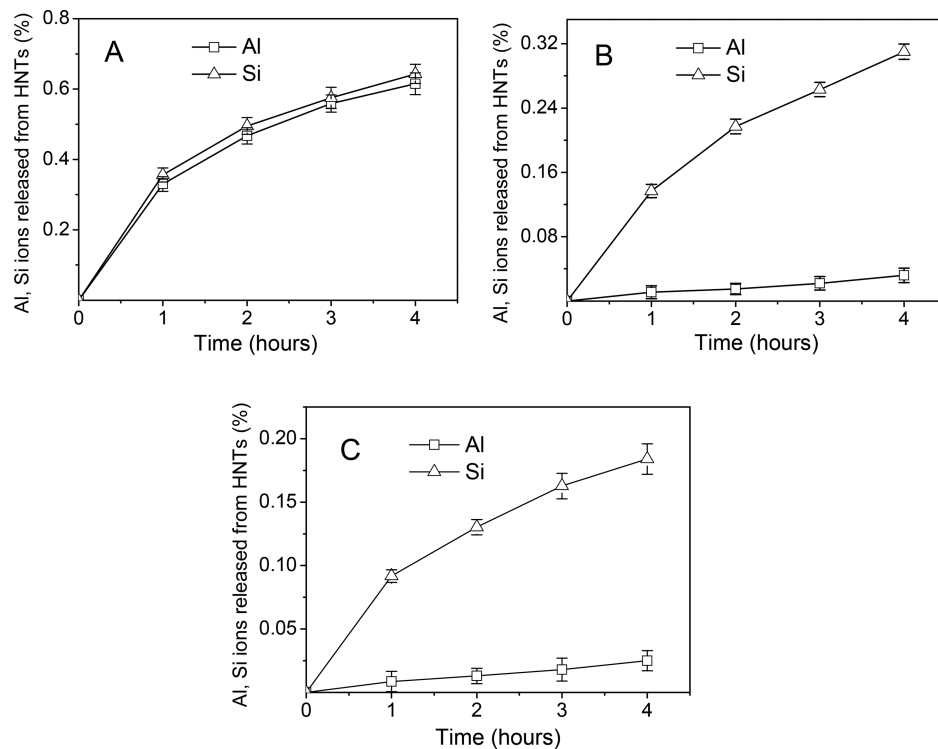


Figure 2. Stability of HNTs in biological conditions. ICP-AES was used to analyze the percentage of dissolution of Al and Si ions after incubation of HNTs with AGF (A), AIF (B), and ABS (C). The experiments of solubility of HNTs were repeated four times. Data were shown as means \pm SD ($n = 4$).

while the mice exhibited changes such as passive behavior and loss of appetite in the high dose group (50 mg/kg BW). Interestingly, as shown in Figure 4A, the body weight in low-

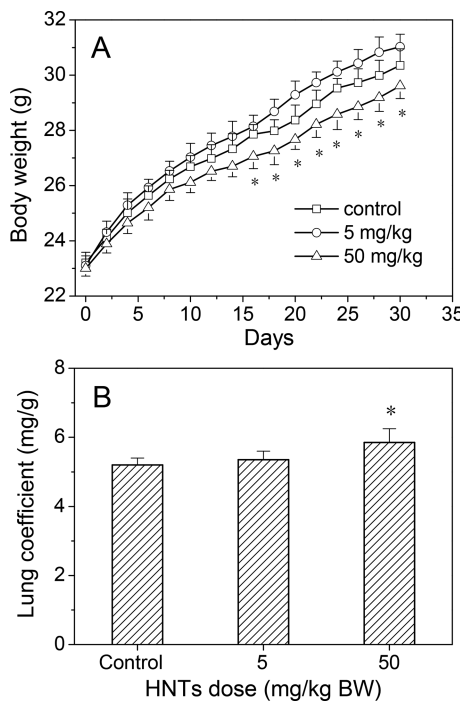


Figure 4. Body weight and coefficient of mouse lung. The increase in mouse body weight during the experimental process (A) and coefficient of the lung after intragastric administration of HNTs for 30 days (B). Data are shown as means \pm SD ($n = 10$). * $p < 0.05$ versus the control.

dose group increased faster than the control, while in high-dose group the body weight increased more slowly than that in the control, indicating that HNTs stimulated the growth of the mice at the low dose but inhibited the growth of the mice at the high dose. The lung coefficient was measured and shown in Figure 4B. No significant change was found in lung coefficients between the control group and the low-dose group ($p > 0.05$), whereas the lung coefficient was markedly higher in the high dose group than that in the control ($p < 0.05$), suggesting that HNTs might cause injury in the lung at high dose.

Contents of Al and Si in the lung. Interestingly, oral administration of HNTs for 30 days had different effects on the biodistributions of Al and Si in the lung (Figure 5A,B). The contents of Al and Si in the lung increased with increasing administration doses of HNTs. However, the Al accumulation in the lung was much higher than that of Si in the high dose group, which might be attributed to the different dissolution rates of Al and Si ions in HNTs in the lung. The pH value of the lung tissue was 7.4.³³ The dissolution rate of Si ions in HNTs was much higher than that of Al ions at 7.4 (Figure 2C). The dissolved Si ions re-entered into the systemic circulation and excreted from the body. In contrast, dissolution of Al ions in HNTs was very slow and majority of the Al ions in HNTs remained insoluble in the lung tissue. Previous work showed that absorbed Si in humans was rapidly excreted in the urine,³⁴ but the expulsion of accumulated Al from the lungs of rats was quite slow.³⁵ The different biodistributions of Al and Si in the lung might be caused by the different excretion rates of Al and Si. On the other hand, HNTs-induced accumulation of Al in

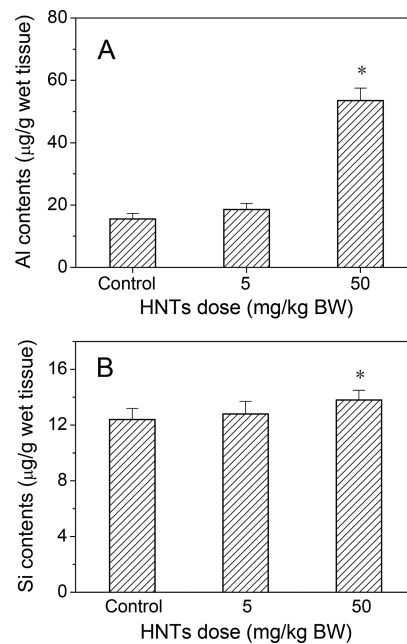


Figure 5. Contents of Al (A) and Si (B) in the lung measured with ICP-AES. Mice were orally administrated with HNTs for 30 days. Data are shown as means \pm SD, $n = 4$. * $p < 0.05$ versus the control.

the lung might be also attributed to the dissolution of Al ions in HNTs in gastric fluid and intestinal fluid. These Al ions entered the blood by the uptake of gastrointestinal tract and accumulated in the lung.

Histopathological Evaluation. Figure 6 shows the histological changes in the pulmonary tissues. The pulmonary tissues in control group showed normal lung architecture (Figure 6A). Administration of 5 mg/kg BW HNTs did not cause observable histological changes (Figure 6B), revealing that HNTs at the low dose had no adverse effects on the lung. However, in the high dose group, exudation of red cells, inflammatory cell infiltration and small areas of fibrosis were observed in the pulmonary tissue (Figure 6C). The exudation of red cells in alveolar space suggested the increase of the permeability of the alveolar capillary membrane. The spindle nuclei and pink collagen fibers indicated fibrosis in the lung tissue (Figure 6D).

Deposition of HNTs. Interestingly, it was discovered that in the high dose group, light blue particles were deposited in the pulmonary tissues (Figure 7C,D). Almost all areas of inflammatory cell infiltration and fibrosis had the light blue particles while it was rare to find such particles in the normal alveolus. The light blue particles were found in the lungs of majority of the mice in the high dose group. These light blue particles were analyzed by confocal Raman microscopy. As shown in Figure 7E, the Raman spectral bands of these particles were very similar to that of the purified HNTs. Both particles in the lung and the purified HNTs had the same characteristic peaks at 133 nm (O-Si-O bend of Si_2O_5 unit on the outside surface), 159 nm (O-Al-O symmetric bend of the AlO_6 octahedral on the inner surface), 209 nm (O-H-O symmetric bend), 699 nm (ν_1 mode of SiO_4), 819 nm (Si-O-Al deformation), 945 nm (Al-OH libration) and 1087 nm (Si-O stretch) (Figure 7F). The results indicate that the particles in the lung were HNTs and essentially retained the natural structure of HNTs. The normal pulmonary tissues did not show these Raman spectral bands. The deposition of the

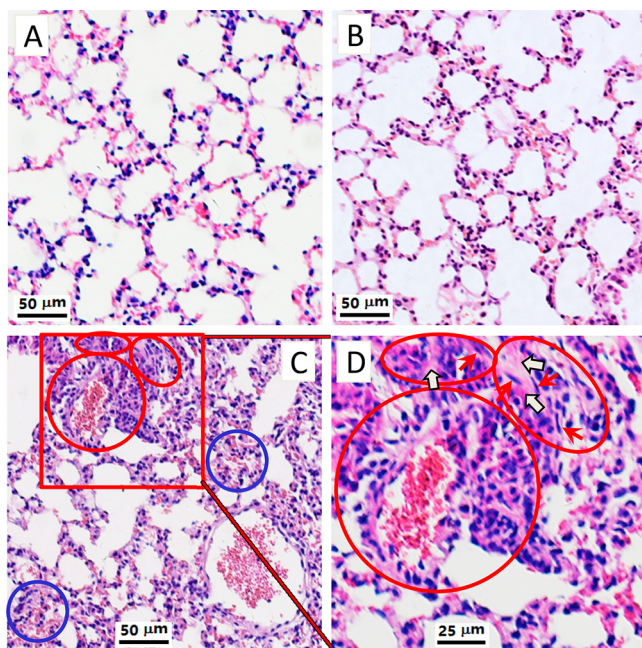


Figure 6. Histopathological observations of pulmonary tissue sections after oral administration of HNTs for 30 days: (A) normal pulmonary alveoli in the control group; (B) 5 mg/kg group shows normal pulmonary alveoli; (C) 50 mg/kg group shows exudation of red blood cells (blue circles), inflammatory cell infiltration (red circle) and fibrosis (red ellipses); (D) high magnification area denoted by rectangle in panel C shows proliferation of alveolar epithelial cells (red circle), fibrosis (red ellipses), spindle nuclei (solid red arrows), and pink collagen fibers (hollow arrows).

particles of HNTs was not found in the lung in the control and low dose groups (Figure 7A,B).

HNTs-Induced Oxidative Stress. The influence of oral HNTs on oxidative stress in pulmonary tissue was assessed by measuring the endogenous antioxidative enzymes, SOD, and GSH-Px in the lung. It was reported that the low levels of antioxidant enzymes would result in the high levels of oxygen free radical production.³⁶ Figure 8A shows that compared to the control, the GSH-Px activity did not vary in the low-dose group ($p > 0.05$) but reduced significantly in the high-dose group ($p < 0.05$). However, administration of HNTs did not cause significant changes in SOD activity ($p > 0.05$) in the lung in all dose groups (Figure 8B).

The level of MDA in the lung was determined and shown in Figure 8C. Compared to the control group, administration of HNTs did not induce a marked change ($p > 0.05$) in MDA level in the lung at the low dose but caused a marked increase ($p < 0.05$) in the MDA level in the lung at the high dose. These results together indicate that administration with HNTs did not cause oxidative stress in the lung at the low dose but induced significant oxidative stress in the lung at the high dose, which might be attributed to the high accumulation of Al and deposition of HNTs in the organ.

HNTs-Induced Expression of iNOS and COX-2. To analyze the HNTs-induced inflammatory response in the lung, the levels of two indicators of inflammation, iNOS and COX-2, were determined by ELISA. As shown in Figure 9A,B, administration of HNTs did not induce significant changes ($p > 0.05$) in the iNOS and COX-2 levels in the lung at the low dose but led to significant increases ($p < 0.05$) in the iNOS and COX-2 levels in the lung at the high dose, which confirmed that

oral HNTs induced inflammatory response in the lung at the high dose.

DISCUSSION

HNTs have been considered to be “green” environmentally safe materials.²² Many studies on *in vitro* toxicity of HNTs showed that HNTs exhibited very low cytotoxicity at moderate levels of exposure.^{21–23} Liu et al. showed that pristine HNTs exhibited little toxicity in *E. coli*.³⁷ However, Choi et al. reported that the pristine HNTs exhibited high toxicity toward *E. coli*.³⁸ These ambiguous results might be caused by the side effects of impurities in pristine HNTs. In the present study, the purified HNTs have been used to precisely predict the toxicity of HNTs by eliminating side effects of impurities. It was found that oral administration of HNTs had opposite effects on the growth of the mice at different doses: stimulating the growth of the mice at the low dose but inhibiting the growth of the mice at the high dose (Figure 4A). Taylor et al.²⁰ revealed that cloisite, clay-based nanoparticle, could elevate the growth of *S. typhimurium*, and because of that cloisite contains some beneficial trace mineral components. HNTs also contain trace mineral components, such as Fe, Mg, and Ca (Table 1), which might also play a role in stimulation of mouse growth.

It was found that nanoparticles could reach the systemic circulation after intravenous or injection inhalation.³⁹ In this study, it was observed that HNTs were deposited in the lung tissues in the high dose group (Figure 7C,D), indicating that oral HNTs could be absorbed from gastrointestinal tract into blood and finally reached the lung. Lee et al. reported that when were administered orally, the oral nanoparticles could be absorbed by the stomach and transported into the systemic circulation.^{40,41} Three possibilities of uptake by the gastrointestinal tract have been suggested by Kreuter: (1) lymphatic uptake, (2) intracellular uptake, and (3) uptake via paracellular pathway.⁴² Li et al. showed that after entering the systemic circulation, the nanoparticles became primarily associated with hepatic Kupffer cells and pulmonary alveolar macrophages.^{40,43} The particles of HNTs were observed only in the lung tissue and they were not found in the other organs, such as the kidney, brain, heart, liver, and spleen, even at the high dose (data not shown). These results reveal that the HNTs in the systemic circulation were primarily taken up by the pulmonary alveolar macrophage. Lung is the most sensitive organ to the materials with high aspect ratio, such as asbestos and carbon nanotube.^{44–46} The present data also showed the lung as the main target organ of oral HNTs with high aspect ratio. Although the detailed picture of the translocation pathway of HNTs to the lung cannot be inferred from the present data, it is certain that the HNTs could be transported from the gastrointestinal tract to the lung. Further investigation is necessary to clarify the mechanism of the translocation of HNTs to the lung.

Interestingly, oral administration of HNTs had different influences on the Al and Si biodistributions in the mice: significantly increasing Al content in the lung with a relative slight increase in Si content in the lung, which were attributed to the different dissolution rates of Al and Si ions in HNTs in the lung and the different excretion rates of Al and Si. After oral administration, HNTs underwent slight dissolution in the gastrointestinal tract, most of which were not dissolved in the gastrointestinal tract. Some of the undissolved HNTs were absorbed from the gastrointestinal tract into blood and finally reached the lung, whereas other undissolved HNTs were finally

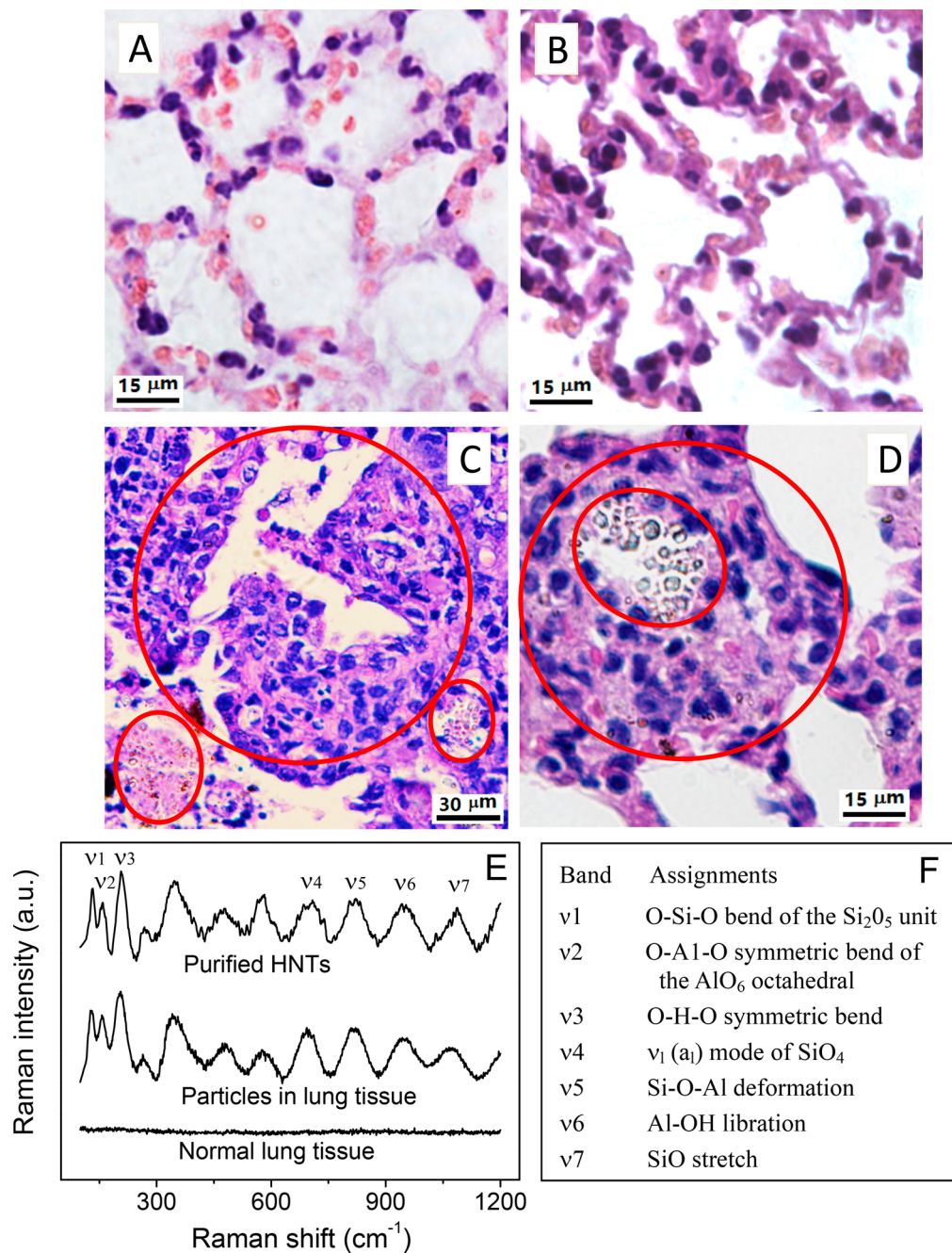


Figure 7. Deposition of HNTs in histopathological sections of the lung tissue. The mice were intragastrically administrated with HNTs for 30 days: (A) normal pulmonary alveoli in control group; (B) 5 mg/kg group shows normal pulmonary alveoli without light blue particles; (C and D) 50 mg/kg group shows light blue particles (ellipse) and inflammatory cell infiltration (circles); (E) Raman spectra of the purified HNTs, normal lung tissue, and light blue particles in panel D; (F) band assignments of Raman spectrum of the purified HNTs in panel E according to the works of Frost and Shurvell.³⁷

eliminated via feces. The HNTs in the lung also underwent slight dissolution. Because the dissolution rate of Si ions in HNTs was much higher than that of Al ions at pH 7.4 (Figure 2C), majority of Si ions in some HNTs in the lung would dissolve and re-entered into the systemic circulation, while the majority of the Al ions in some HNTs remained insoluble in the lung tissue, resulting in the significant Al accumulation in the lung. Because the expulsion of Si ions from the lung was much faster than that of Al ions,^{34,35} only slight Si accumulation was observed in the lung.

It is well-known that exposure to the materials with high aspect ratio, such as asbestos⁴⁷ and carbon nanotubes,⁴⁸ can induce the lung fibrosis in animals. From the present results, oral HNTs with high aspect ratio also induced the fibrosis in the lung in the high-dose group. The fibrosis was caused by the particles of HNTs, based on the fact that the particles of HNTs were deposited almost in all areas of fibrosis and such particles were rarely found in the normal alveolus (Figure 7). Kommireddy et al.⁴⁹ found that HNTs stimulated the growth of human dermal fibroblasts. The present results also show that the deposited HNTs stimulated the growth of fibroblasts and

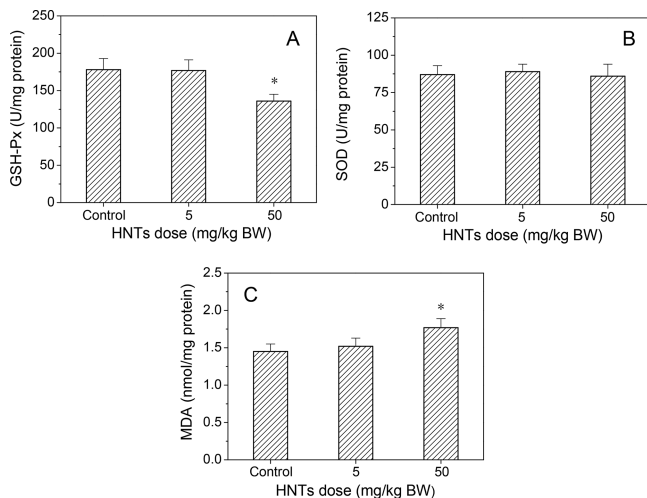


Figure 8. GSH-Px activity (A) and the SOD activity (B), and the MDA level (C) in the mouse lung after oral administration of HNTs for 30 days. Data are shown as means \pm SD, $n = 4$. * $p < 0.05$ versus the control.

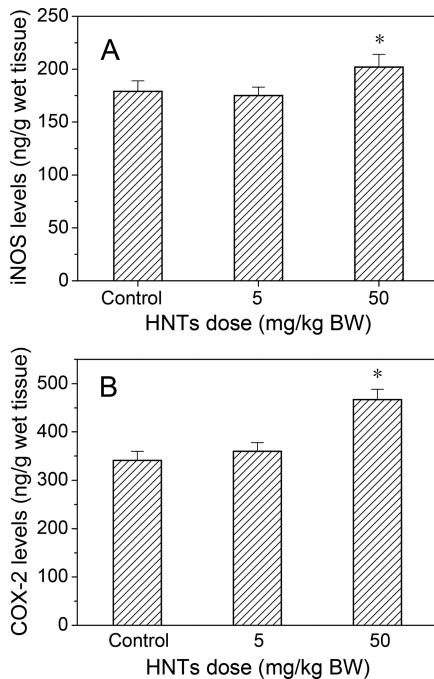


Figure 9. Levels of iNOS and COX-2 in the mouse lung after oral administration of HNTs for 30 days. Data are shown as means \pm SD, $n = 4$. * $p < 0.05$ versus the control.

increased collagen synthesis by fibroblasts and caused pulmonary fibrosis (Figure 6D). On the other hand, chronic inflammation is considered as the cause of fibrogenesis. Therefore, the pulmonary fibrosis also results from oral HNTs-induced inflammatory cell infiltration.

Previous works indicated that the Al accumulation in lung did not cause pulmonary fibrosis.³² Pauluhn et al.⁵⁰ showed that inhalation of Al(OH)₃ nanoparticles at a concentration of 28 mg/m³ for 28 days did not cause pulmonary fibrosis in rats. Buraimoh et al.⁵¹ showed that oral AlCl₃ at doses of 475, 950, 1425, or 1900 mg/kg BW for 8 weeks did not induce fibrosis in the pulmonary tissues of rats in all AlCl₃ treated groups. Taylor et al.⁵² revealed that coating of carbon nanotube with Al₂O₃

could reduce carbon nanotubes-induced mouse lung fibrosis. These results together suggest that HNTs-induced pulmonary fibrosis was not caused by Al accumulation.

The external surfaces of HNTs exposure to media are silica, thus the toxicity of HNTs may be compared with that of SiO₂ nanoparticle.²¹ Both HNTs and silica nanoparticles can induce reactive oxygen species.⁵³ The surface interactions of the nanoparticles with media can directly produce reactive oxygen species. The Fe ions on the surface of the nanotubes also produce reactive oxygen species by the Fenton reaction.⁵⁴ The purified HNTs contained a small amount of iron (Table 1). Because Fe ion acts as a catalyst in Fenton reaction,⁵⁴ a few Fe ions in HNTs can cause the generation of large amount of ROS, which can lead to oxidative stress and lipid peroxidation in the lung (Figure 8). On the other hand, Kaneko et al.⁵⁵ reported that orally administrated AlCl₃ induced pulmonary oxidative stress. Therefore, the pulmonary oxidative stress might be caused not only by deposited HNTs but also by accumulated Al in the organ.

The HNTs-induced pulmonary oxidative stress at the high dose caused significant increases in COX-2 and iNOS levels in the pulmonary tissues. COX-2 is one important enzyme that is involved in the process of inflammation, and its expression is highly inducible in various tissues by inflammatory cytokine stimuli.⁵⁶ iNOS is an inflammatory factor, and the increased iNOS expression leads to the inflammatory response.⁵⁷ The marked increases in the COX-2 and iNOS levels in the lung at the high dose indicate oral HNTs-induced pulmonary inflammation, which is consistent with the histopathological abnormalities in the lung.

The concentrations of HNTs in different environments are variable. People may be exposed to HNTs at different doses in different situations. The doses of HNTs were used in the present study according to the suggestion of the OECD Guidelines 420.³¹ The dose does not must reflect its real concentration in actual environments, whereas, our result may be used to assess the effects of the environments with severe contamination of HNTs on human health. The results also indicate the safety of HNTs in the applications in mice at low doses (5 mg/kg BW). In a regular biomedical application in human beings, the oral dosages of HNTs are usually lower than 5 mg/kg BW. Yin et al.¹⁶ reported that addition of HNTs to zearalenone-contaminated diets at a dose of 0.1 g/kg could diminish the negative effects of zearalenone in swine. On the basis of the current results, caution should be taken when applying HNTs at such a high dose (0.1 g/kg BW).

In summary, oral administration of HNTs stimulated the growth of the mice at low dose with no pulmonary toxicity but inhibited the growth of the mice and induced oxidative stress in the lung at high dose. HNTs had high stability in biological conditions. Oral administration of HNTs significantly increased Al content but did not markedly affect Si content in the lung. This study provides the first evidence that oral HNTs at high dose could be absorbed from gastrointestinal tract and deposited in lung and could also induce pulmonary fibrosis. Our findings will be of benefit in understanding the effects of HNTs on the respiratory system.

AUTHOR INFORMATION

Corresponding Author

*E-mail: xuxl@ustc.edu.cn.

ORCID®

Xiaolong Xu: 0000-0002-9997-4483

Funding

This study was supported by grants from the National Natural Science Foundation of China (Grants 20571069, 20871111, and 21171157).

Notes

The authors declare no competing financial interest.

ABBREVIATIONS USED

HNTs, halloysite nanotubes; BW, body weight; TEM, transmission electron microscopy; XRF, X-ray fluorescence; DLS, dynamic light scattering instrument; ROS, reactive oxygen species; MDA, malondialdehyde; SOD, superoxide dismutase; ICP-AES, inductively coupled plasma-atomic emission spectrometry; GSH-Px, glutathione peroxidase; COX-2, cyclooxygenase-2; iNOS, nitric oxide synthase; AGF, artificial gastric fluid; AIF, artificial intestinal fluid; ABS, artificial blood solution

REFERENCES

- (1) Bates, T. F.; Hildebrand, F. A.; Swineford, A. Morphology and structure of endellite and halloysite. *Am. Mineral.* **1950**, *35*, 463–484.
- (2) Massaro, M.; Lazzara, G.; Milioto, S.; Noto, R.; Riela, S. Covalently modified halloysite clay nanotubes: synthesis, properties, biological and medical applications. *J. Mater. Chem. B* **2017**, *5*, 2867–2882.
- (3) Massaro, M.; Riela, S.; Guernelli, S.; Parisi, F.; Lazzara, G.; Baschieri, A.; Valgimigli, L.; Amorati, R. A synergic nanoantioxidant based on covalently modified halloysite-trolox nanotubes with intralumen loaded quercetin. *J. Mater. Chem. B* **2016**, *4*, 2229–2241.
- (4) Wilson, M. J. Clay Mineralogical and Related Characteristics of Geophagic Materials. *J. Chem. Ecol.* **2003**, *29*, 1525–1547.
- (5) Wilson, I. R. Kaolin and halloysite deposits of China. *Clay Miner.* **2004**, *39*, 1–15.
- (6) Peng, Q.; Liu, M.; Zheng, J.; Zhou, C. Adsorption of dyes in aqueous solutions by chitosan–halloysite nanotubes composite hydrogel beads. *Microporous Mesoporous Mater.* **2015**, *201*, 190–201.
- (7) Wang, L.; Chen, J. L.; Ge, L.; Zhu, Z. H.; Rudolph, V. Halloysite-Nanotube-Supported Ru Nanoparticles for Ammonia Catalytic Decomposition to Produce CO_x-Free Hydrogen. *Energy Fuels* **2011**, *25*, 3408–3416.
- (8) Massaro, M.; Colletti, C. G.; Lazzara, G.; Milioto, S.; Noto, R.; Riela, S. Halloysite nanotubes as support for metal-based catalysts. *J. Mater. Chem. A* **2017**, *5*, 13276–13293.
- (9) Lvov, Y.; Wang, W.; Zhang, L.; Fakhrullin, R. Halloysite Clay Nanotubes for Loading and Sustained Release of Functional Compounds. *Adv. Mater.* **2016**, *28*, 1227–1250.
- (10) Liang, W.; Wu, Y.; Sun, H.; Zhu, Z.; Chen, P.; Yang, B.; Li, A. Halloysite clay nanotubes based phase change material composites with excellent thermal stability for energy saving and storage. *RSC Adv.* **2016**, *6*, 19669–19675.
- (11) Massaro, M.; Riela, S.; Baiamonte, C.; Blanco, J. L. J.; Giordano, C.; Lo Meo, P.; Milioto, S.; Noto, R.; Parisi, F.; Pizzolanti, G.; Lazzara, G. Dual drug-loaded halloysite hybrid-based glycocluster for sustained release of hydrophobic molecules. *RSC Adv.* **2016**, *6*, 87935–87944.
- (12) Rizzo, C.; Arrigo, R.; D'Anna, F.; Di Blasi, F.; Dintcheva, N. T.; Lazzara, G.; Parisi, F.; Riela, S.; Spinelli, G.; Massaro, M. Hybrid supramolecular gels of Fmoc-F/halloysite nanotubes: systems for sustained release of camptothecin. *J. Mater. Chem. B* **2017**, *5*, 3217–3229.
- (13) Tas, C.; Hendessi, S.; Baysal, M.; Unal, S.; Cebeci, F.; Menceloglu, Y.; Unal, H. Halloysite Nanotubes/Polyethylene Nano-composites for Active Food Packaging Materials with Ethylene Scavenging and Gas Barrier Properties. *Food Bioprocess Technol.* **2017**, *10*, 789–798.
- (14) Biddeci, G.; Cavallaro, G.; Di Blasi, F.; Lazzara, G.; Massaro, M.; Milioto, S.; Parisi, F.; Riela, S.; Spinelli, G. Halloysite nanotubes loaded with peppermint essential oil as filler for functional biopolymer film. *Carbohydr. Polym.* **2016**, *152*, 548–557.
- (15) Liu, M.; Zhu, D.; Guo, T.; Zhang, Y.; Shi, B.; Shan, A.; Chen, Z. Toxicity of zearalenone on the intestines of pregnant sows and their offspring and alleviation with modified halloysite nanotubes. *J. Sci. Food Agric.* **2018**, *98*, 698.
- (16) Yin, S.; Meng, Q.; Zhang, B.; Shi, B.; Shan, A.; Li, Z. Alleviation of zearalenone toxicity by modified halloysite nanotubes in the immune response of swine. *Food Addit. Contam., Part A* **2015**, *32*, 87–99.
- (17) Zhang, Y.; Gao, R.; Liu, M.; Yan, C.; Shan, A. Adsorption of modified halloysite nanotubes in vitro and the protective effect in rats exposed to zearalenone. *Arch. Anim. Nutr.* **2014**, *68*, 320–335.
- (18) Nair, R.; Varghese, S. H.; Nair, B. G.; Maekawa, T.; Yoshida, Y.; Kumar, D. S. Nanoparticulate material delivery to plants. *Plant Sci.* **2010**, *179*, 154–163.
- (19) Chichiriccò, G.; Poma, A. Penetration and Toxicity of Nanomaterials in Higher Plants. *Nanomaterials* **2015**, *5*, 851–873.
- (20) Taylor, A. A.; Aron, G. M.; Beall, G. W.; Dharmasiri, N.; Zhang, Y.; McLean, R. J. Carbon and clay nanoparticles induce minimal stress responses in gram negative bacteria and eukaryotic fish cells. *Environ. Toxicol.* **2014**, *29*, 961–8.
- (21) Vergaro, V.; Abdullayev, E.; Lvov, Y. M.; Zeitoun, A.; Cingolani, R.; Rinaldi, R.; Leporatti, S. Cytocompatibility and Uptake of Halloysite Clay Nanotubes. *Biomacromolecules* **2010**, *11*, 820–826.
- (22) Lai, X.; Agarwal, M.; Lvov, Y. M.; Pachpande, C.; Varahramyan, K.; Witzmann, F. A. Proteomic profiling of halloysite clay nanotube exposure in intestinal cell co-culture. *J. Appl. Toxicol.* **2013**, *33*, 1316–1329.
- (23) Ahmed, F. R.; Shoaib, M. H.; Azhar, M.; Um, S. H.; Yousuf, R. I.; Hashmi, S.; Dar, A. In-vitro assessment of cytotoxicity of halloysite nanotubes against HepG2, HCT116 and human peripheral blood lymphocytes. *Colloids Surf., B* **2015**, *135*, 50–55.
- (24) Bellani, L.; Giorgetti, L.; Riela, S.; Lazzara, G.; Scialabba, A.; Massaro, M. Ecotoxicity of halloysite nanotube-supported palladium nanoparticles in *Raphanus sativus* L. *Environ. Toxicol. Chem.* **2016**, *35*, 2503–2510.
- (25) Fakhrullina, G. I.; Akhatova, F. S.; Lvov, Y. M.; Fakhrullin, R. F. Toxicity of halloysite clay nanotubes in vivo: a *Caenorhabditis elegans* study. *Environ. Sci.: Nano* **2015**, *2*, 54–59.
- (26) Kryuchkova, M.; Danilushkina, A.; Lvov, Y.; Fakhrullin, R. Evaluation of toxicity of nanoclays and graphene oxide in vivo: a *Paramecium caudatum* study. *Environ. Sci.: Nano* **2016**, *3*, 442–452.
- (27) Rong, R.; Xu, X. L.; Zhu, S. S.; Li, B.; Wang, X.; Tang, K. B. Facile preparation of homogeneous and length controllable halloysite nanotubes by ultrasonic scission and uniform viscosity centrifugation. *Chem. Eng. J.* **2016**, *291*, 20–29.
- (28) Delaval, M.; Boland, S.; Solhonne, B.; Nicola, M. A.; Mornet, S.; Baeza-Squiban, A.; Sallenave, J. M.; Garcia-Verdugo, I. Acute exposure to silica nanoparticles enhances mortality and increases lung permeability in a mouse model of *Pseudomonas aeruginosa* pneumonia. *Part. Fibre Toxicol.* **2015**, *12*, 1.
- (29) Zhu, S.; Xu, X.; Rong, R.; Li, B.; Wang, X. Evaluation of zinc-doped magnetite nanoparticle toxicity in the liver and kidney of mice after sub-chronic intragastric administration. *Toxicol. Res.* **2016**, *5*, 97–106.
- (30) Yan, X.; Rong, R.; Zhu, S.; Guo, M.; Gao, S.; Wang, S.; Xu, X. Effects of ZnO Nanoparticles on Dimethoate-Induced Toxicity in Mice. *J. Agric. Food Chem.* **2015**, *63*, 8292–8.
- (31) OECD. *Guideline for testing of chemicals. Acute oral toxicity—fixed dose procedure*. Adopted December 17, 2001.
- (32) Park, E. J.; Kim, H.; Kim, Y.; Choi, K. Repeated-dose toxicity attributed to aluminum nanoparticles following 28-day oral administration, particularly on gene expression in mouse brain. *Toxicol. Environ. Chem.* **2011**, *93*, 120–133.
- (33) Adamcakova-Dodd, A.; Stebounova, L. V.; Kim, J. S.; Vorink, S. U.; Ault, A. P.; O'Shaughnessy, P. T.; Grassian, V. H.; Thorne, P. S.

- Toxicity assessment of zinc oxide nanoparticles using sub-acute and sub-chronic murine inhalation models. *Part. Fibre Toxicol.* **2014**, *11*, 15.
- (34) Dobbie, J. W.; Smith, M. J. B. Urinary and Serum Silicon in Normal and Uremic Individuals. *Ciba Found. Symp.* **2007**, *121*, 194–213.
- (35) Schlesinger, R. B.; Snyder, C. A.; Chen, L. C.; Gorczynski, J. E.; Menache, M. Clearance and translocation of aluminum oxide (alumina) from the lungs. *Inhalation Toxicol.* **2000**, *12*, 927–939.
- (36) Xu, B.; Xu, Z. F.; Deng, Y.; Yang, J. H. Protective effects of Chlorpromazine and Verapamil against cadmium-induced kidney damage in vivo. *Exp. Toxicol. Pathol.* **2010**, *62*, 27–34.
- (37) Zhang, Y.; Chen, Y.; Zhang, H.; Zhang, B.; Liu, J. Potent antibacterial activity of a novel silver nanoparticle-halloysite nanotube nanocomposite powder. *J. Inorg. Biochem.* **2013**, *118*, 59–64.
- (38) Choi, H. J.; Stazak, T. J.; Montemagno, C. D. Surface-dependent cytotoxicity on bacteria as a model for environmental stress of halloysite nanotubes. *J. Nanopart. Res.* **2013**, *15*, 2008.
- (39) Pujalte, I.; Passagne, I.; Brouillaud, B.; Treguer, M.; Durand, E.; Ohayon-Courtes, C.; L'Azou, B. Cytotoxicity and oxidative stress induced by different metallic nanoparticles on human kidney cells. *Part. Fibre Toxicol.* **2011**, *8*, 10.
- (40) Lee, C. M.; Jeong, H. J.; Yun, K. N.; Kim, D. W.; Sohn, M. H.; Lee, J. K.; Jeong, J.; Lim, S. T. Optical imaging to trace near infrared fluorescent zinc oxide nanoparticles following oral exposure. *Int. J. Nanomed.* **2012**, *7*, 3203–3209.
- (41) Eldridge, J. H.; Hammond, C. J.; Meulbroek, J. A.; Staas, J. K.; Gilley, R. M.; Tice, T. R. Controlled Vaccine Release in the Gut-Associated Lymphoid-Tissues 0.1. Orally-Administered Biodegradable Microspheres Target the Peyer's Patches. *J. Controlled Release* **1990**, *11*, 205–214.
- (42) Kreuter, J. Peroral Administration of Nanoparticles. *Adv. Drug Delivery Rev.* **1991**, *7*, 71–86.
- (43) Li, C. H.; Shen, C. C.; Cheng, Y. W.; Huang, S. H.; Wu, C. C.; Kao, C. C.; Liao, J. W.; Kang, J. J. Organ biodistribution, clearance, and genotoxicity of orally administered zinc oxide nanoparticles in mice. *Nanotoxicology* **2012**, *6*, 746–756.
- (44) Boulanger, G.; Andujar, P.; Pairon, J. C.; Billon-Galland, M. A.; Dion, C.; Dumortier, P.; Brochard, P.; Sobaszek, A.; Bartsch, P.; Paris, C.; Jaurand, M. C. Quantification of short and long asbestos fibers to assess asbestos exposure: a review of fiber size toxicity. *Environ. Health* **2014**, *13*, 59.
- (45) Donaldson, Murphy; Schinwald; Duffin; Poland. Identifying the pulmonary hazard of high aspect ratio nanoparticles to enable their safety-by-design. *Nanomedicine* **2011**, *6*, 143–156.
- (46) Yang, S.-t.; Guo, W.; Lin, Y.; Deng, X.-y.; Wang, H.-f.; Sun, H.-f.; Liu, Y.-f.; Wang, X.; Wang, W.; Chen, M.; Huang, Y.-p.; Sun, Y.-P. Biodistribution of Pristine Single-Walled Carbon Nanotubes In Vivo. *J. Phys. Chem. C* **2007**, *111*, 17761–17764.
- (47) Boulanger, G.; Andujar, P.; Pairon, J. C.; Billon-Galland, M. A.; Dion, C.; Dumortier, P.; Brochard, P.; Sobaszek, A.; Bartsch, P.; Paris, C.; Jaurand, M. C. Quantification of short and long asbestos fibers to assess asbestos exposure: a review of fiber size toxicity. *Environ. Health* **2014**, *13*, 59.
- (48) Vietti, G.; Lison, D.; van den Brule, S. Mechanisms of lung fibrosis induced by carbon nanotubes: towards an Adverse Outcome Pathway (AOP). *Part. Fibre Toxicol.* **2015**, *13*, 11.
- (49) Kommireddy, D. S.; Ichinose, I.; Lvov, Y. M.; Mills, D. K. Nanoparticle Multilayers: Surface Modification for Cell Attachment and Growth. *J. Biomed. Nanotechnol.* **2005**, *1*, 286–290.
- (50) Pauluhn, J. Pulmonary toxicity and fate of agglomerated 10 and 40 nm aluminum oxyhydroxides following 4-week inhalation exposure of rats: toxic effects are determined by agglomerated, not primary particle size. *Toxicol. Sci.* **2009**, *109*, 152–67.
- (51) Buraimoh, A. A.; Ojo, S. A. Effects of aluminium chloride exposure on the histology of lungs of wistar rats. *J. Appl. Pharm. Sci.* **2013**, *3*, 108–112.
- (52) Taylor, A. J.; McClure, C. D.; Shipkowski, K. A.; Thompson, E. A.; Hussain, S.; Garantziotis, S.; Parsons, G. N.; Bonner, J. C. Atomic layer deposition coating of carbon nanotubes with aluminum oxide alters pro-fibrogenic cytokine expression by human mononuclear phagocytes in vitro and reduces lung fibrosis in mice in vivo. *PLoS One* **2014**, *9*, e106870.
- (53) Petushkov, A.; Ndiege, N.; Salem, A. K.; Larsen, S. C. Toxicity of silica nanomaterials: zeolites, mesoporous silica, and amorphous silica nanoparticles. *Advances in Molecular Toxicology* **2010**, *4*, 223–266.
- (54) Singh, N.; Jenkins, G. J.; Asadi, R.; Doak, S. H. Potential toxicity of superparamagnetic iron oxide nanoparticles (SPION). *Nano Rev.* **2010**, *1*, 5358.
- (55) Kaneko, N.; Yasui, H.; Takada, J.; Suzuki, K.; Sakurai, H. Orally administrated aluminum-maltolate complex enhances oxidative stress in the organs of mice. *J. Inorg. Biochem.* **2004**, *98*, 2022–31.
- (56) Kuwano, T.; Nakao, S.; Yamamoto, H.; Tsuneyoshi, M.; Yamamoto, T.; Kuwano, M.; Ono, M. Cyclooxygenase 2 is a key enzyme for inflammatory cytokine-induced angiogenesis. *FASEB J.* **2004**, *18*, 300–310.
- (57) Lipton, S. A.; Choi, Y. B.; Pan, Z. H.; Lei, S. Z.; Chen, H. S.; Sucher, N. J.; Loscalzo, J.; Singel, D. J.; Stamler, J. S. A redox-based mechanism for the neuroprotective and neurodestructive effects of nitric oxide and related nitroso-compounds. *Nature* **1993**, *364*, 626–32.